Marine and Petroleum Geology 26 (2009) 1724–1739

Contents lists available at ScienceDirect

Marine and Petroleum Geology

journal homepage: www.elsevier.com/locate/marpetgeo

Modeling study of growth and potential geohazard for LUSI mud volcano: East Java, Indonesia

Bambang P. Istadi [a,*], Gatot H. Pramono [b], Prihadi Sumintadireja [c], Syamsu Alam [d]

[a] Energi Mega Persada., Wisma Mulia 22nd Floor, Jl. Jend. Gatot Subroto 42, 12710 Jakarta, Indonesia
[b] Bakosurtanal, Jl. Jakarta-Bogor Km. 46, 16911 Cibinong, Indonesia
[c] Applied Geology Research Division, Institute of Technology Bandung, Jl. Ganesha 10, Bandung 40132, Indonesia
[d] Pertamina EP, J. Prof. Dr. Satrio No. 164, Jakarta 12950, Indonesia

ARTICLE INFO

Article history:
Received 11 April 2008
Received in revised form
19 March 2009
Accepted 23 March 2009
Available online 5 April 2009

Keywords:
Mud volcano
LUSI
Modeling
Simulation
Geohazard

ABSTRACT

The mud volcano known as LUSI first erupted in May 2006 in East Java, Indonesia. The eruption has continued for over two years, and potentially will continue for many years to come, impacting an ever larger area. An obvious and significant question is how extensive the impacted area will become in the coming years. The answer is important for planning scenarios for the relocation of people and infrastructure and for managing the environment and economy. To make such a prediction, an understanding of the geological processes controlling the mud volcanic evolution is needed.

A three-dimensional simulation model was built to predict the area affected by the mudflow over a ten-year period, with a special focus on the period from December 2007 until June 2010. The primary model inputs are the mud debit rate, the rate of subsidence and the topography. The model prediction was validated at the December 2007 time step by comparing the results with satellite images from the same period. The simulation was found to provide a good approximation for the mud overflow and growth. The results indicate that the mudflow tends to spread to the west and particularly to the east and north from the currently inundated area. The model predicts that in June 2010 the peak of the mud volcano will have risen 26 m above the original ground level, and the maximum subsidence will have been −63 m below the original ground level. The dynamic subsurface condition in the area creates geohazard risks, and these are also discussed in this paper.

1. Introduction

The mud eruption occurred in May 2006 in at least five separate locations forming a NNE–SSW lineament about 200 m away from the Banjarpanji-1 (BJP-1) exploration well in Sidoarjo, approximately 30 km south of Surabaya, East Java, Indonesia (Fig. 1). The approximately 700 m lineament is contiguous with the Watukosek fault zone. Some 50,000 m^3/day of hot mud was erupting in the initial months. In September 2006, the eruption rate escalated to 125,000 m^3/day and reached a maximum of 156,000 m^3/day before decreasing to the rate of approximately 90,000 m^3/day at the time of writing this paper in August 2008.

The cause of the mud eruption is still in debate (i.e. Mazzini et al., 2007; Davies et al., 2007, 2008; Tingay et al., 2008; Sawolo et al., 2008, 2009; Istadi et al., 2008) and consequently so is the solution to the problem. If the mud eruption stems from an underground blowout, then in theory it can be stopped by drilling relief well(s) to intersect the original Banjarpanji-1 hole and then pumping heavy mud followed by cement. However, if the mud eruption is up reactivated faults with no connection to the wellbore, then it is impossible to stop the eruption.

Initially, given the proximity of the eruption to the well, the general public assumed that the mudflow was caused by an underground blowout from the Banjarpanji-1 well. Later, after the full field data set was carefully integrated and analyzed, it became clear from both field data and pressure analysis that the well and the mud eruption are unconnected (Sawolo et al., 2008, 2009). Firstly, the wellbore fluid pressure was too low to fracture the wellbore. Secondly, there was no sustained wellbore fluid pressure to propagate the fractures to surface, as the BOP was left in the open position. Thirdly, the wellbore was open and totally dead whilst mud was erupting at 50,000 m^3/day only 200 m away (Istadi et al., 2008). The most likely trigger for the mudflow was the reactivation of the Watukosek fault system (Mazzini et al., 2007), in which case the mud eruption cannot be stopped, and is predicted to flow for decades.

* Corresponding author. Tel.: +62 8 1188 3266.
E-mail address: bambang.istadi@energi-mp.com (B.P. Istadi).

0264-8172/$ – see front matter © 2009 Elsevier Ltd. All rights reserved.
doi:10.1016/j.marpetgeo.2009.03.006

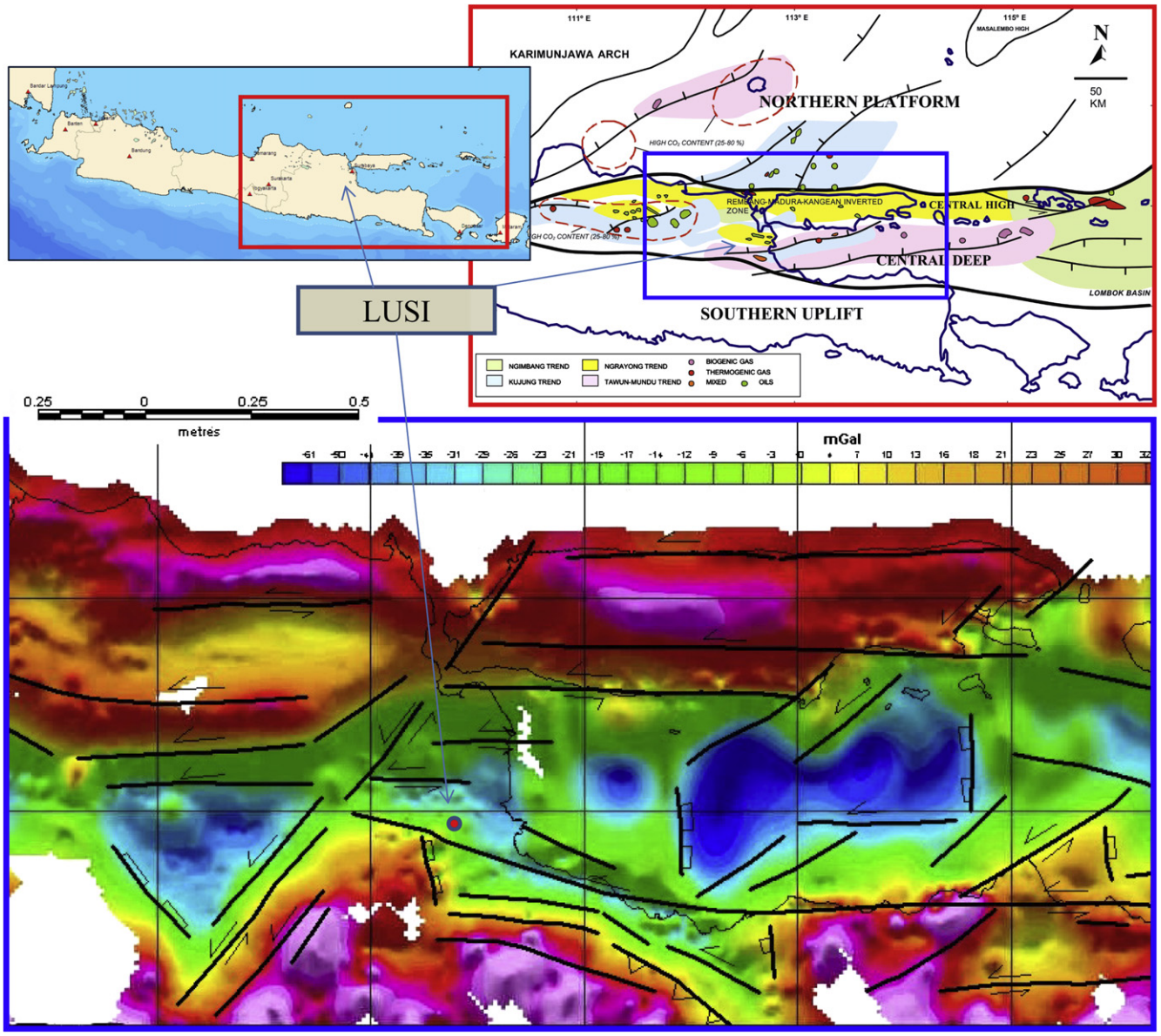

Fig. 1. LUSI is located in East Java, about 30 km South of Surabaya (top left). Regional tectonic framework of East Java (top right) shows major NE–SW and E–W major fault trends. Bouguer gravity map (processed with 2.65 g/cc density) of East Java (bottom) showing East Java Basin's depositional centers (blue) which are controlled by the major faults in the area. (For interpretation of the references to color in this figure legend, the reader is referred to the web version of this article.)

Many studies have been conducted on existing mud volcanoes, but little is known about the geological conditions prior to and during the initial stages of mud volcanic eruptions. LUSI is special, as the evolving geological processes from LUSI's birth can be observed. This paper addresses the potential impact and related geohazard risks from the continued mud eruption in the years to come, and can be used as a reference to other mud volcanoes.

2. General geology

Several models have been proposed to describe the complexity of the East Java Basin, among others van Bemmelen (1949), De Genevraye and Samuel (1972), Hamilton (1979), Hall (2002), Sribudiyani et al. (2003), Smyth et al. (2005), and Prasetyadi et al. (2006). The East Java Basin developed as a back-arc basin as a result of the northwestward subduction of the Australian oceanic plate below the Sunda continent during the Late Cretaceous time. A major extensional tectonic system prevailed during the Early Tertiary time caused by complex interactions between the Australian, Eurasian and Pacific plates. This created extensional graben systems and the development of rift basins. These series of half-grabens developed and aligned along Pre-Tertiary NE–SW lines of weakness, shifting to an E–W direction further to the South. These two distinctive trends are recognized as the structural configuration of the East Java Basin. The NE trending faults create the most prominent structural grain, interpreted as the plate boundary fault trend that was inherited from the Cretaceous subduction zone and accretionary prism. The second major fault trend developed within the Southern part of the Basin bordered by Northern Fold Belt, where the major sub-basins are defined by E–W trending faults, and depocenters are aligned parallel to the Madura Island and northern coast of the East Java Island. The NE–SW orientation, forming structural lows of various sub-basins is stretched from the offshore Java Sea towards the onshore part of the East Java Area (Fig. 1).

The basement configuration has a NE–SW structural orientation and comprises a series of well defined basement ridges with intervening grabens serving as depocenters, which contain Tertiary sediments. Clastic sediment deposition and carbonate buildup of the Ngimbang Formation took place during the Eocene and Early Oligocene. The Late Oligocene and Miocene sequence is separated from the underlying sequence by an unconformity which served as the foundation of ENE–WSW oriented carbonate trends. This platform development, which is known as the Kujung limestone, occurred in the late Oligocene while the Prupuh and Tuban reefal development took place in the Early to Middle Miocene. The latest and most pronounced period of compressional tectonism began in the Late Miocene time and continued episodically into the Pleistocene. The resulting transpressional regime caused left-lateral movement that runs East–West that resulted in an East–West orientation of the anticline structures.

Subsequent Pliocene and Pleistocene sedimentation consisted of an Eastward-prograding mudstone-dominated volcaniclastic wedge of Kalibeng and Pucangan Formation, with a thickness of ~2400–3000 m. The volcaniclastic materials are derived from the Java volcanic arc south of the Sidoarjo area. The mudstone of the Kalibeng Formation is over-pressured in most parts of the basin where rapid pressure transition occurs. The high sedimentation rate, rapid deposition and burial of thick shale in the depocenters that occurred during Pliocene and Pleistocene have resulted in zones of under-compacted shales (Willumsen and Schiller, 1994; Schiller et al., 1994). This highly plastic zone is over-pressured due to the presence of excessive trapped water and maturing organic rich materials. The many mud volcanoes found in East and Central Java correlate with this thick and rapidly deposited clay-bearing Kalibeng Formation sediments. At least four known naturally occurring mud volcanoes exist around LUSI out of the 14 identified in East and Central Java (Fig. 2).

The active tectonics coupled with over-pressured maturing organic rich sediments makes East Java an ideal setting for mud volcanism. The existence of the NE–SW trending Watukosek fault system in the LUSI area provides the necessary conduit for mud, fluid and gases extruding from a deep horizon to flow up to the surface to form the LUSI mud volcano (Fig. 3).

3. Geohazard risks

The mud eruption in Sidoarjo has buried houses, villages, schools, factories, and displaced thousands of people and continues to pose geohazard risks in a densely populated area with many activities and infrastructures. This modeling study of growth and potential geohazard is a part of the risks anticipation and planning for the worst case scenario within the LUSI mud volcano and its surrounding areas.

Studies of other mud volcanoes in East Java were used in geohazard assessment. The still active Bleduk Kuwu mud volcano in Central Java (Fig. 2) consists of a mud volcano complex with multiple mud eruption sites in a radius of 3.5 km from the main mud eruption suggesting the presence of several active conduits. LUSI had five mud eruption vents initially, but only one remains active. There is a possibility that inactive mud eruption vents may reactivate or new ones will emerge in other locations. The study suggests a possibility of mud erupting at one or more of the known gas bubble locations or at a new location along zones of weakness on reactivated pre-existing faults or on new fault zones.

Methane gas bubbles have been identified in more than 90 locations, and are generally associated with fractures. Some are more active than others while some have died. In most cases, the methane is non-flammable only because it is in such low concentrations from rapid dispersion in the air. However where bubbles are confined, the concentration of methane is high enough to burn. The gas leaks from these fractures suggest breach of seal and loss of sealing capacity of faults and the impervious shale overlying geological structures that contain gas accumulations. The occurrence of gas bubbles also suggests that subsidence is not merely

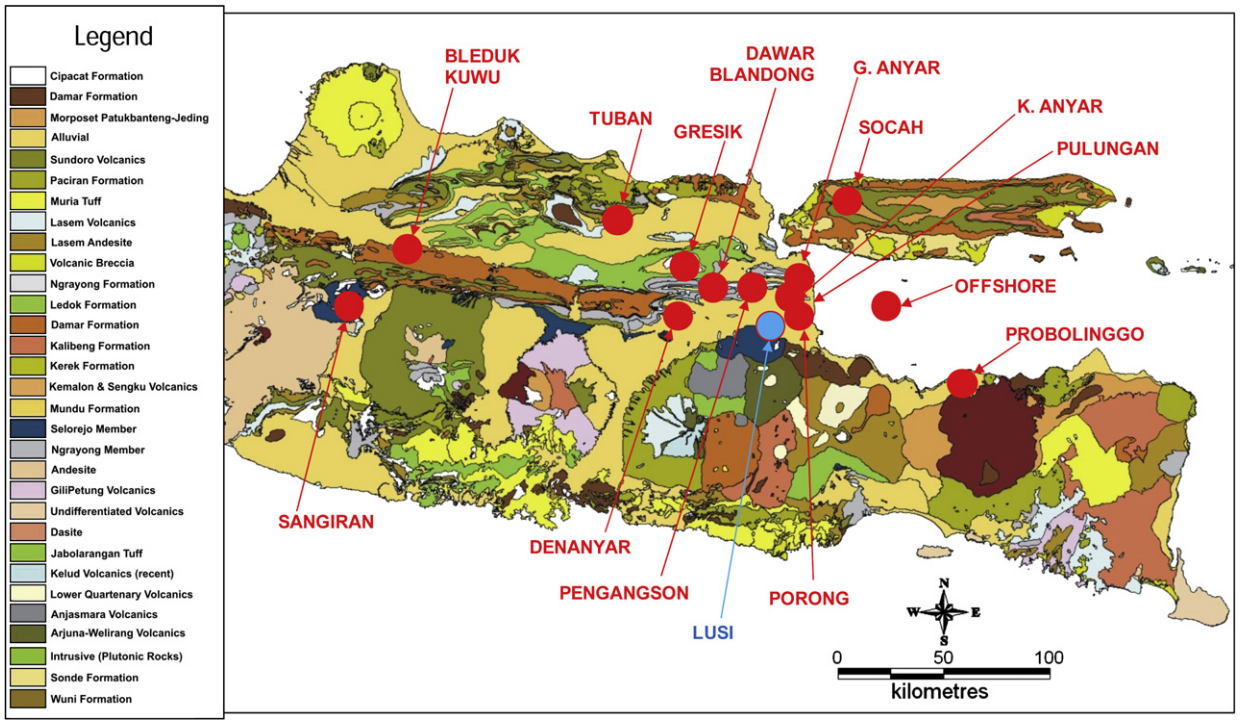

Fig. 2. Geological map and mud volcano distribution in East and Central Java. Red dots are the identified mud volcano locations. Some are used as analogs for LUSI mud volcano model development. (Map modified after Gafoer and Ratman, 1999.) (For interpretation of the references to color in this figure legend, the reader is referred to the web version of this article.)

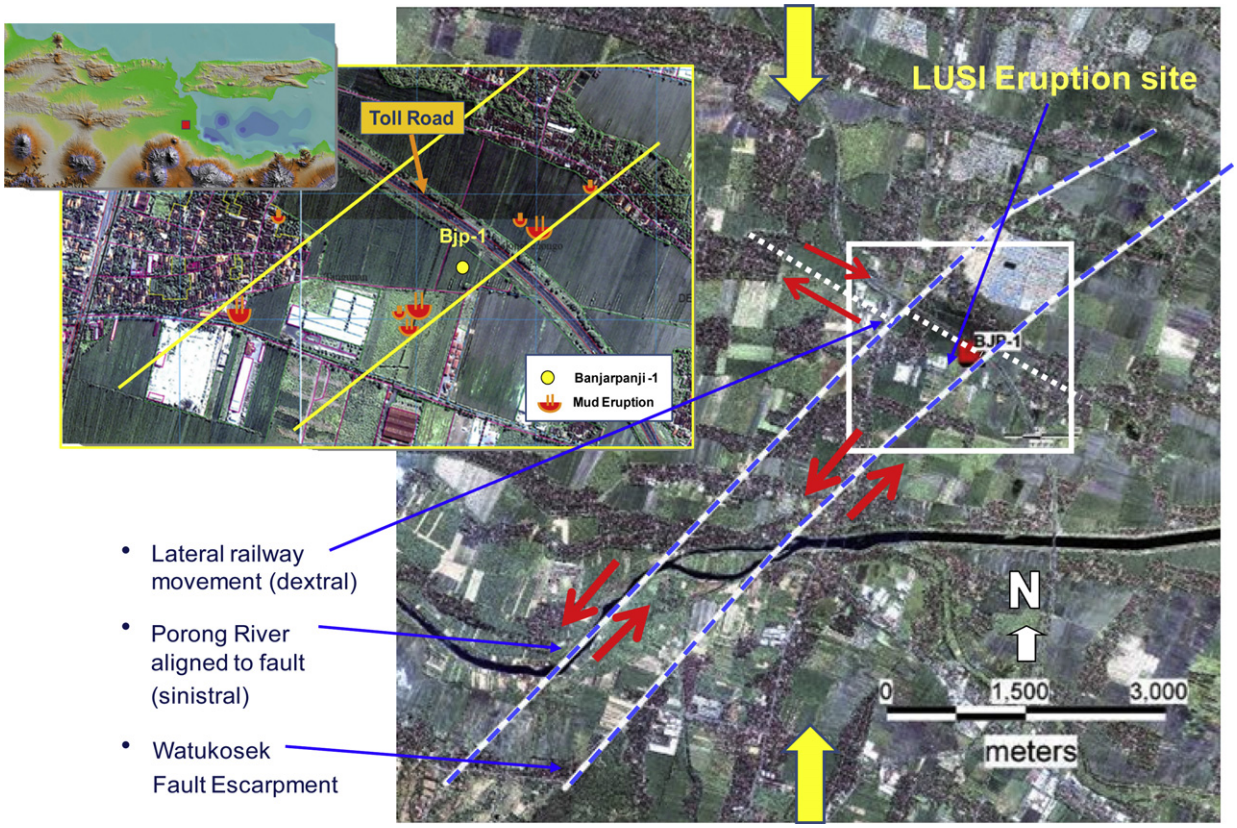

Fig. 3. Watukosek fault, consisting of 2 parallel faults where Porong River is aligned along the fault line, while the Watukosek fault escapement represents the up thrown fault block. LUSI eruption sites are along the Watukosek fault line.

a shallow near-surface phenomenon as a result of surface loading by the weight of the mud or soft soil layer compaction, but instead also affecting deep horizons as the gas comes from a deep source. Gas chromatography of sampled gas bubbles near the main eruption vent in July 2006 indicates it primarily consists of methane but the presence of some heavier gases in small quantities including ethane, propane, butane, and pentane suggest a deep thermogenic origin and long extended fractures.

A particular area of concern in the area is the faults reactivation, where differential movement has created shear stress. Areas within a 2–3 km radius of the main mud eruption vent are experiencing ongoing horizontal and vertical movement aligned to faults. The displacements have spatial and temporal variations in magnitude and direction (Fig. 3). The resulting fractures from reactivation of pre-existing faults or newly formed faults have damaged houses, buildings and nearby infrastructure. Such movement is evident in the dextral movements of a railway in September 2006 where the fault displacements are more than the GPS-measured subsidence movement. The bursting of a gas pipeline and numerous breakages of water pipelines at the same location further supports displacements along faults. The continued movements along faults would likely result in the emergence of more gas bubbles.

Continuing subsidence in the form of a depression bowl or cone is occurring due to the continued mud eruption. The subsidence forms accommodation space, a natural basin to contain the mud. The high water content of the mud (~70–60% water and slurry) means the mud has low viscosity and therefore cannot accumulate vertically and form a high and steep mountain-like structure. The mud tends to spread sideways which increases pressure on the mud retaining dikes, which could collapse and cause flooding.

The area faces risk of flooding as the mud affected area expands. Dikes and levees were constructed as temporary mud containment in an emergency situation; they were constructed simply from soil and rock matrix and are unstable. The collapse of dikes in the past has resulted in flooding of hot mud (ranging about 85–95 °C) and caused injury to human and animals. Future dike failures are likely as the mud buildups grow and exert increasing hydrostatic pressure on the dike walls. As the risk of future dike failure is high, therefore alternative public transport routes should be prepared to maintain accessibility.

In terms of geohazard risks, the evidence and areas of concern include i) rupture of gas and water pipelines (shear and subsidence); ii) railroad bending (shear/faulting and subsidence); iii) road cracks (subsidence); iv) relief wells casing integrity (subsidence and shear); v) dike collapse (subsidence); v) gas bubbles which appear along fractures and zones of weakness (shear/faulting and subsidence).

4. Stopping the mudflow

Several attempts using various methods and techniques to stop the mud eruption were carried out. At least four methods have been applied to stop the mudflow. The first was Snubbing Unit method (re-entry of the Banjarpanji-1 well), followed by Well Side Tracking method, then the use of Relief Wells, and the last was High Density Chained Balls (HDCB) method. These attempts faced many safety issues and subsurface challenges without any success. The chances of stopping the mudflow are slim, even if the mud eruption were stopped successfully, there is a high probability that new mud eruptions would appear elsewhere. Indeed, another mud eruption started along the Watukosek fault plane (about 1 km) to the South of LUSI in September 2006, during the second microgravity survey. The mudflow is still going strong, currently erupting at approximately 90,000 m^3/day at the time of writing this paper.

Important geological information about LUSI was gained from previous relief wells (RW-1 and RW-2) drilled to stop the mud eruption. The relief wells operations were conducted between June 2006 and January 2007 and revealed the dynamic geological conditions of the LUSI mud volcano discussed below:

- Mud eruption comes from a fault plane not from the wellbore. RW-1 well penetrated a fault plane and suffered continual drilling mud losses and kicks. As the subsurface condition deteriorates, the fault networks are reactivated and formed. On the other hand the BJP-1 well did not intersect any faults and drilling fluid was able to circulate even after the mud eruptions had appeared.
- The increasingly active fault network has resulted in more gas bubbles in the area. Some suddenly appeared close to relief well(s) which could pose a danger and compromise the safety of the crew and equipment for the relief well(s) operation.
- At the beginning of the re-entry operations of the BJP-1 well, there were no problems, but as subsidence and horizontal movement progressed, problems began. Subsidence and horizontal movement have caused tight hole, key seating, equipment failure, casing collapse and buckling, moving upwards from deep to shallow zones in BJP-1 well as well as RW-1 and RW-2 wells. Even a wellhead drop was observed. Casing integrity was difficult to achieve as deformation progressed. The movements involve shallow as well as deep horizons as the casing collapse suggest.
- The safety of relief well operations depended on the integrity of the dikes preventing the mud from flooding the drilling area. However as pressure increases on the dikes, they collapsed, causing flooding of hot mud. Differential movements along the faults have caused cracks and displacements resulting in dikes collapse in the past.

As there is no indication that the mudflow would stop anytime soon and attempts to stop the mudflow were not successful, consequently understanding the geohazard risks becomes important. Predicting the risks and area which could be affected by the ongoing mud eruption and subsidence is essential for the planning for the people and facilities. Studies and surveys are needed to understand the behavior of this mud volcano and in building a predictive model.

5. Surveys and studies

Several surveys and studies were conducted by Lapindo Brantas (the oil company who was blamed for causing the mudflow by drilling the Banjarpanji-1 exploration well), in collaboration with various universities and institutions to gain a better understanding of the geological processes and areal extent and potential impact of the mudflow. The research and field surveys included studies on nearby mud volcanoes in East Java, aerial photography, gravity and microgravity, resistivity, very-low frequency (VLF) electromagnetic, micro-seismic, GPS (Global Positioning System) and geohazard monitoring (Sumintadireja et al., 2007). Studies on geochemistry, paleontology, geothermal, hydrology, water chemistry, mineralogy, gas compositions and isotopes helped to determine the source of the mud, water and gas.

The erupted mud is sourced from "bluish gray clay" of the Upper Kalibeng Formation, which is Pleistocene in age and deposited in a middle to outer shelf environment (Kadar et al., 2007). Based on paleontological analyses of the Banjarpanji-1 well, it was also found that the mud at the surface comes from a depth of 1554 to 1920 m. This finding is consistent with geochemical correlation, i) The Kerogen profile of the mud is consistent with that from cuttings and side-wall cores taken at a depth of 1707 m and ii) The thermal maturity profile (vitrinite reflectance) is also consistent with cuttings and side-wall cores (Istadi et al., 2008). The presence of under-compacted overpressured shale is evident from Banjarpanji-1 logs, and the reactivation of faults provides the conduit for the mud to flow to the surface.

The surveys relevant to understand and map the deformation of the LUSI area are discussed below.

5.1. Geodetic surveys

Geodetic measurements were conducted at the LUSI site to quantify the ongoing deformation processes. The primary data sources were the GPS surveys periodically conducted at monitoring stations to measure vertical and horizontal movements relative to a more stable reference station. Seven GPS survey campaigns were conducted between June 2006 and April 2007. The GPS measurements were conducted at 33 locations using dual-frequency geodetic type receivers over various time intervals. Each measurement lasted from 5 to 7 h. Continuous GPS subsidence monitoring was conducted at the two relief well locations (Fig. 4).

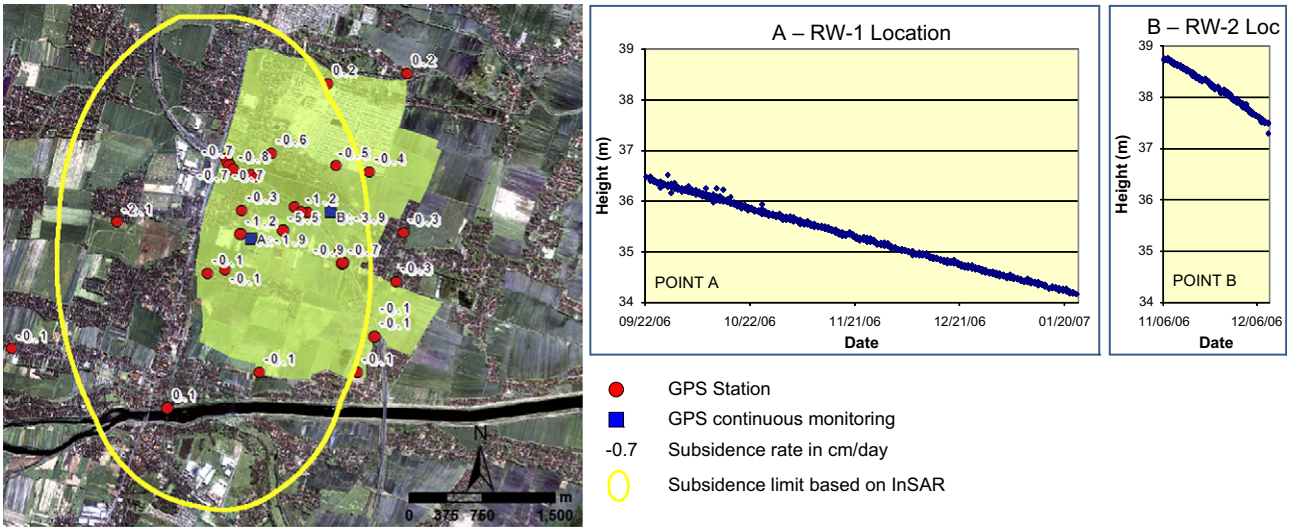

Fig. 4. The subsidence was measured by GPS at 33 locations. Two selected GPS continuous measurements (highlighted A and B) are plotted to illustrate the mean subsidence rates of 1.9 and 3.9 cm/day for RW-1 and RW-2 locations respectively. The yellow ellipse represents the interpreted subsiding area based on InSAR Satellite data processing. (For interpretation of the references to color in this figure legend, the reader is referred to the web version of this article.)

The survey data indicated that horizontal and vertical displacements have indeed occurred relative to the more stable reference station, with subsidence rates between 1 cm/day and 5 cm/day up to 3 km from the main mud eruption vent.

The GPS data were complemented by Trigonometry Leveling at two reference points near LUSI. This data is less precise (in both angle and distance measurement) because the reference points were themselves likely affected by subsidence. Never-the-less, to monitor the stability of the relief well rigs, it was sufficiently accurate. Measurements were carried out daily, mainly at 15 perimeter points around the relief wells. The measurements were tied weekly to Bakosurtanal Benchmark reference points. The measurements indicated that up to 92 cm of subsidence occurred within a 33-day period.

A Real Time Kinematic (RTK) survey was carried out on a daily basis with two reference points near the eruption vent to monitor the integrity of the dikes and to estimate the mud volume. This survey was not intended to monitor subsidence.

Despite the less accurate measurements, the latter two geodetic surveys were nonetheless useful to validate the GPS monitoring data.

5.2. Mud dimensions and volumes

Understanding the mudflow dimensions was necessary to calculate the mud eruption rate, which was a key input into the simulation model. Field Surveys were carried out in June and July 2006 at 51 locations to measure the area inundated by mud. The mudflow height was measured using measuring tape by comparison with the adjacent unflooded area. The extent of the flooded area was computed using the IKONOS satellite image. The area and thickness was used to calculate the volume and average mudflow rate over the one-month interval. The survey was repeated in May 2007, with 42 survey points in order to quantify the change in mud dimension, volume and eruption rate a year after the start of the eruption.

The mud volume was computed using a Geographic Information System (GIS) package with the capability of performing three-dimensional analyses. The volume calculation used the cut-and-fill method that calculates volumes where material has been removed or gained (Hogan, 1973). The approach was used by Price (2002) and Pendrod et al. (2006). The volume computation is based on five-by-five meter grid cells. The volume for each cell (V) is obtained from

$$V = h^{*}A_{\text{cell}} \tag{1}$$

where h = height and A_{cell} = area of a grid cell which is 25 m^2.

The mud height for each cell was interpolated from measured values using the nearest-neighbor approach, as this resulted in values within the range of measured points.

For the months of June and July 2006, the mud-flooded areas were 111 hectares and 179 hectares respectively, while the calculated mud volumes were 1.1 million m^3 and 2.5 million m^3 respectively (Pramono and Sardjono, 2007). The same approach was applied in May 2007. Despite the partial containment of the mud expansion by dikes, the mud-flooded area had increased to 628 hectares, more than five times greater than the flooded area in June 2006, whilst the calculated mud volume had increased to about 37.3 million m^3.

5.3. Gravity

A gravity survey was conducted over the LUSI area in June 2006, three weeks after the mud started to erupt in order to obtain deep subsurface information and possibly identify the presence of mud diapir and its geometry based on density contrast. Mud diapir, however, was not found or penetrated at the Banjarpanji-1 well location. Gravimeter instruments used in the survey were of the mass-spring type system, capable of measuring changes in the Earth's gravitational acceleration down to 1 part in 100 million. This translates into a precision of about 0.01 mgal (1 mgal = 10^{-5} ms^{-2}). The gravity base station in the location was established by tying the base station to the nearest standard gravity base station, located at Surabaya's Juanda airport approximately 12 km North of LUSI. The data was corrected for instrument drift, ellipsoid gravity value, free air and the Bouguer effect using a density of 2.67 g/cc, which is the average basement density value of East Java Basin. In addition, all the 215 observation points were surveyed by handheld GPS. The gravity survey covers 2 km^2 area and 6 km along the toll road with a distance of 100 m apart between measurement stations.

The detailed gravity data results in a good data match with the already compiled regional gravity data for East Java Area (Fig. 1). The Bouguer anomaly map generated for the LUSI area was created using a density of 2.67 g/cc so that the density contrast is relative to this background value. The residual Bouguer anomaly therefore reflects both density contrast in the LUSI area and structural changes represented by dense gravity contour change. The generated residual Bouguer anomaly map confirms the existence of the depocenters, as indicated by lower Bouguer values to the Northeast of LUSI (Figs. 1 and 5). This observation is confirmed by the Bouguer anomaly map, which exhibits the same regional trend. Interestingly, the residual Bouguer anomaly map for shallow strata demonstrates lower values around the LUSI eruption vent and higher values to the Northeast (Fig. 5). The boundary between low and high residual Bouguer anomaly values is interpreted as a fault zone with a normal/strike slip component. The low residual Bouguer anomaly values cover an area of about 1.3 km^2 and is interpreted as shallow subsurface structural effect.

5.4. Microgravity

The microgravity survey was conducted using a gravimeter instrument with 1 μgal (=10^{-8} ms^{-2}) precision to understand the mechanism of mudflow from its source, and to possibly determine subsurface volume changes and mud source volumes. This time-lapse survey was designed to detect microgravity anomaly changes in mass or pressure. Both are reflected in surface gravity changes from subsurface mass movement. Microgravity data acquisition around the LUSI area was conducted over three periods between August and October 2006 with an interval between surveys of around nine days. The survey covered approximately a 7 × 7 km^2 area. The measurement stations were 100–400 m apart, with a total of 137 observations points, and all coordinates were recorded by handheld GPS. The combination of gravimetry with GPS data was necessary to back out two contrary effects: Mass intrusion increases gravity, but subsidence and over-pressure reduce gravity. The quality of the gravity data was controlled by applying the closed loop method, and the resulting accuracy was around 0.005 mGal or 5 μGal. Data corrections were applied for drift and tidal effects, while shallow anomaly source effects were removed with a low-pass filter.

Based on the three microgravity surveys, two microgravity time-lapse maps were generated. These maps showed gravity anomaly variation between the surveys due to mass and magnitude changes in the material lying beneath the measuring stations and surrounding areas (Fig. 6). Positive microgravity values suggest mass increase and possible recharge, while negative values suggest mass decrease or mud/fluid withdrawal (Allis and Hunt, 1986). A microgravity change of −3 μGal is equivalent to −1 cm decrease in height. The resolution of the gravity measurement is about

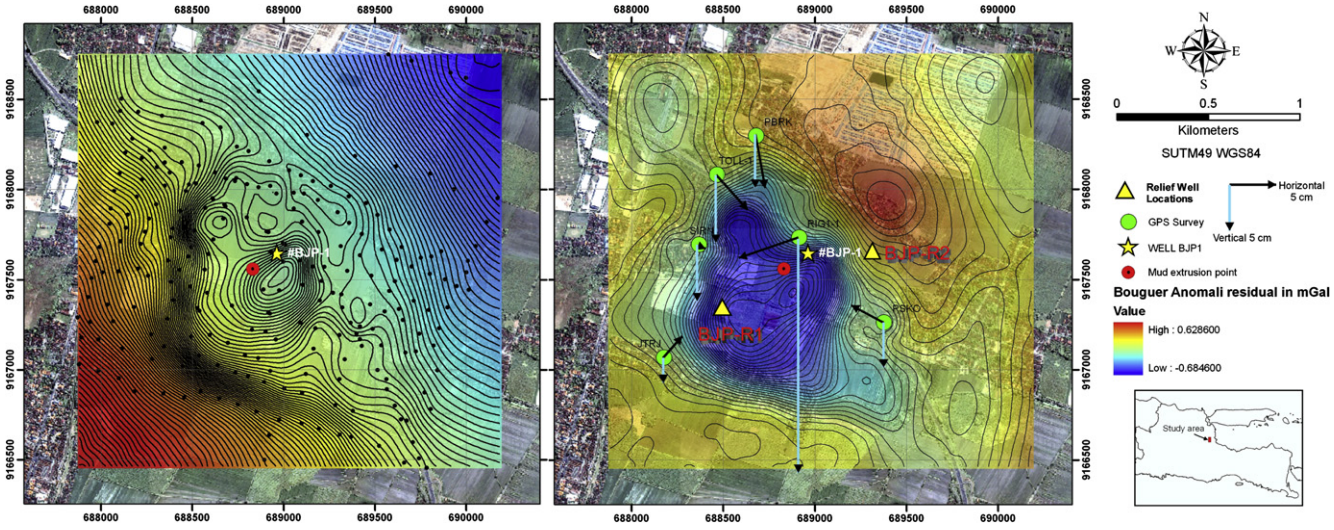

Fig. 5. Bouguer anomaly map (left) shows the existence of the depocenter as indicated by lower Bouguer values to the Northeast of LUSI. The residual gravity data at LUSI (right) and its surrounding area indicate a gravity low, which is interpreted as the subsidence caused by mud withdrawal area, and the presence of faults in high density contrast areas (rapid change in contour). The vertical and horizontal movements marked in light blue and black arrows indicate surface movement direction and magnitude.

$\pm$10 μGal ($\pm$100 nm/s^2) which is equivalent to 3 cm in height (free air gradient) (Jentzsch et al., 1999).

The bulk density changes are interpreted as changes in subsurface conditions due to pressure and density changes that suggest underground mass redistribution caused by remobilization of mass, fluids and gases. The low microgravity values indicate reducing mass at the center of the mud eruption at around 1700 m depth, which is in good agreement with other data sets (see above). This depth was derived from the gravity 2D modeling combined with seismic data in the low-velocity zone and constrained within the well's over-pressured zone. The 2D gravity model uses a Talwani algorithm (Talwani et al., 1959) through forward-modeling to match a calculated body with the observed time-lapse microgravity anomaly.

At the LUSI location increasing negative anomaly values as shown in microgravity time-lapse maps between September 2006–August 2006 and October 2006–August 2006, suggest increasing subsidence caused by increasing mud volume withdrawal (Fig. 6). The negative anomaly also indicates an increasing density contrast with the surrounding area. The increase in time-lapse microgravity with time, i.e. from 150 to 200 μGal is consistent with the increased mud rates during the survey period from 50,000 m^3/day to more than 100,000 m^3/day in September 2006 (see mud eruption section below).

Positive anomalies are distributed in an NE–SW direction that conforms to fault lineaments in this area suggesting that these anomalies are related to mudflow movement along fault planes. The anomaly variations are mainly aligned along the Watukosek fault system which trends NNE–SSW (Fig. 3). The positive anomaly to the NW of the main mud eruption is interpreted as densification process due to withdrawal of low density mud material. The positive anomaly in the southwest area is probably related to low

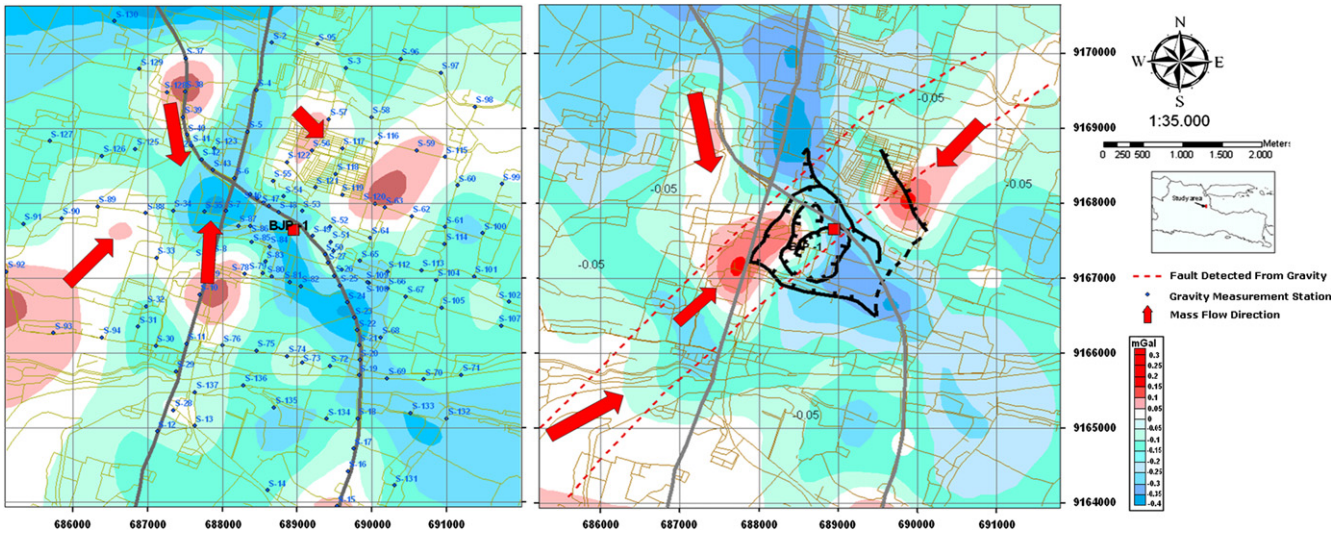

Fig. 6. Microgravity time-lapse anomaly map, September 2006–August 2006 period (left map) and October 2006–August 2006 period (right map). The changes in microgravity patterns over time suggest mass redistribution and mud remobilization, or fluidized over-pressured shale flowing (red arrow) into a conduit plastically along the Watukosek fault lineament (red dotted lines-right map). Positive microgravity values suggest mass increase and recharge, whereas negative values suggest subsidence due to mud/fluid withdrawal. If mountain ranges to the Southwest and areas Northwest recharged the hydrogeological dynamics of LUSI, then the mudflow could last for a very long time.

density material movement and withdrawal where the system could then be recharged from the Arjuno–Welirang volcanic complex to the South of LUSI. If the system is recharged, the volume of recharge is significant since the anomaly is very extensive and reaches a difference of 80 μGal (0.08 mGal) between the micro-gravity time-lapse maps (Fig. 6).

The correlation of microgravity response of 80 μGal is equivalent to a 26 cm elevation change. For the LUSI area it was estimated that 1 μGal response change is equivalent to 18,750 m^3 as the increasing mud eruption rate is approximately 50,000 m^3/day. The volume equivalent to microgravity change is a rough approximation and perhaps can only be applied to LUSI. Additional data points are needed.

5.5. VLF

A VLF (very-low frequency, 15–30 kHz at 10–20 km wavelength) electromagnetic survey was conducted to map shallow faults, as difficult field conditions did not permit acquisition of other types of surveys such as seismic. The VLF survey comprised eight survey lines of differing lengths, oriented roughly South-North and West-East around the mud volcano. Fig. 7 shows one VLF line near the main eruption vent. The Karous–Hjelt filter technique (Karous and Hjelt, 1985) was applied to filter out the high-frequency, low-amplitudes noise which often precedes the VLF signal and which can cause deterioration in the quality of the data.

The VLF revealed the presence of shallow faults in the LUSI area. These faults are in pairs, trending NE–SW but dipping in opposite directions. The Eastern fault dips NW, while the Western fault dips SE. The Eastern fault is interpreted as a synthetic fault of a major fault while the Western fault is interpreted as the antithetic.

5.6. Resistivity

The electrical resistivity survey was carried out to obtain the resistivity contrast around LUSI. Resistivity is a function of porosity, permeability, water saturation and the concentration of dissolved solids in the pore fluids. A resistivity contrast reflects material changes and geological changes in the subsurface, such as the extent of LUSI saline water incursion along the shallow section of the Watukosek fault. The survey was acquired in a profile-sounding mode using a Wenner array configuration (op. cit. Reynolds, 1997). Three lines were acquired, each 700 m long with 10 m electrode spacing.

The result shows a significant resistivity contrast between the western and eastern sides of LUSI. Higher resistivity is more common in the western side ($R > 24\ \Omega$ m), while lower resistivity dominates the eastern side ($R < 1\ \Omega$ m). The conclusion is that the eastern side has conductive layers in both deep and shallow horizons. The low resistivity zones suggest the presence of conductive material such as the saline water component of the LUSI mud (Fig. 7).

6. Mud growth simulation model

A three-dimensional simulation model was built to predict the area affected by the mudflow over a ten-year period, with a special focus on the period December 2007 until June 2010. Multiple data sets and parameters were employed in order to build the model and then to calibrate it, in order to accurately simulate the mudflow. The main controlling parameters in the model are mud eruption rate, subsidence rate and topography. The subsidence pattern is influenced by the fault distribution in the area, so several data sets were employed to determine this, including VLF, resistivity and microgravity anomaly changes. The subsidence area is confined by the inferred subsidence from InSAR (Interferometric Synthetic Aperture Radar) data.

6.1. Mud longevity estimation

The longevity of the mudflow was estimated from the volume of the over-pressured shale formation that could erupt to surface.

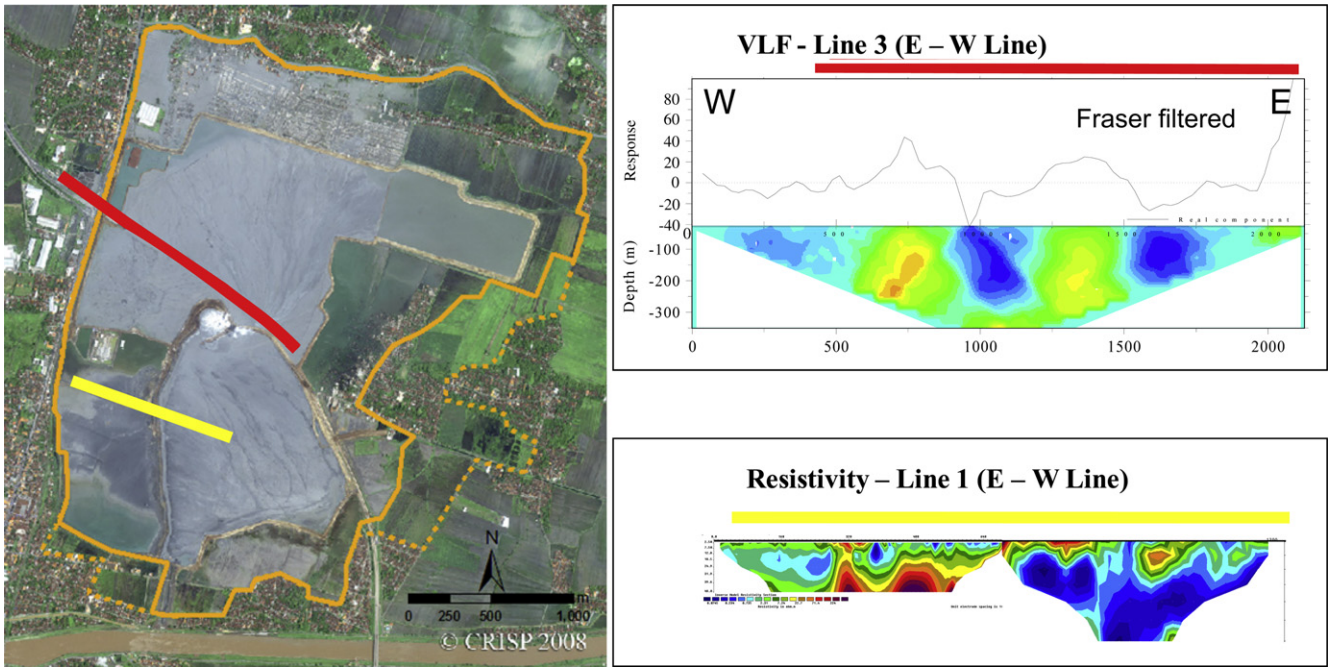

Fig. 7. Initial mud simulation model result for December 2007 (orange dashed line) is validated against the Crisp satellite observation of January 2008. The model over-predicted the mud inundated area and hence the model's inputs were adjusted to match reality. The VLF survey (top right) was along the red line, while the resistivity survey (bottom right) was along the yellow line. Both surveys identified the presence of shallow faults which are covered by swampy soft topsoil. These faults are contiguous with the Watukosek fault system. (For interpretation of the references to color in this figure legend, the reader is referred to the web version of this article.)

The thickness of the over-pressured shale section was derived from the compaction curve which was generated from sonic log data, using the Reiga–Clemenceau equation (Issler, 1992):

$$\varphi = 1 - \left(\frac{t_{ma}}{t_{log}}\right)^{1/x} \quad (2)$$

where φ = porosity, t_{ma} = transit time of the matrix (67.05 μs), t_{log} = transit time from the wireline log and x = acoustic formation factor (2.19).

The compaction curve in the BJP-1 well (Fig. 8) can be divided into three parts. The upper part consists of the Kabuh, Pucangan 1 and Pucangan 2 Formations from 0 to 3220 ft (~980 m), where no data is available, so the burial-history model used compaction curves of Sclater and Christie (1980). The middle part consists of the Upper Kalibeng 1 Formation, where the lithology is dominated by shale, and the compaction curve falls into the category of under-compacted or over-pressured formations. The lower part consists of the Upper Kalibeng 2 Formation, where the lithology is predominantly volcanic sandstone, and the compaction curve falls into the normal compaction range.

The estimated thickness of the over-pressured Kalibeng 1 Formation is 2100 ft (640 m) shown in Fig. 8. This over-pressured zone which is shale dominated interval between 6100 ft and 4000 ft (~1860–1220 m) in Banjarpanji-1 well correlates with the low-velocity zone as shown in the interval velocity profile derived from check-shot data of Banjarpanji-1 well (Fig. 8). Seismically the low-velocity zone is shown in Fig. 9.

The areal extent of the Kalibeng 1 Formation was estimated from two data sources. Seismic data was used by mapping the low-velocity shale layer. Gravity data was used by mapping the low gravity area in the Bouguer residual plot. The areal extent estimates were 2 km^2 and 1.3 km^2 respectively (Fig. 10). This figure also shows the 2D seismic lines acquired in 1991 and 1996 over Banjarpanji-1 and LUSI area.

The longevity of the eruption is the volume (thickness multiplied by the averaged area from the two sources of data) divided by the assumed mud eruption rate of 100,000 m^3/day. The result is that the mud eruption could last from 23 to 35 years. This prediction however depends on the subsurface mass and pressure conditions where a number of factors such as over-pressure shales, seismicity and tectonics influence eruption longevity and flow mechanism. The mudflow will stop sooner if a there is no external charging, and it will flow for longer if the system is being recharged. Another possibility is intermittent flow, where the mudflow stops, the pressure builds up and breaches the overburden, and then the flow starts again.

6.2. Mud eruption rate

The mud eruption rate was a calculation based on field measurements of mud dimensions conducted in 2006 and 2007. The

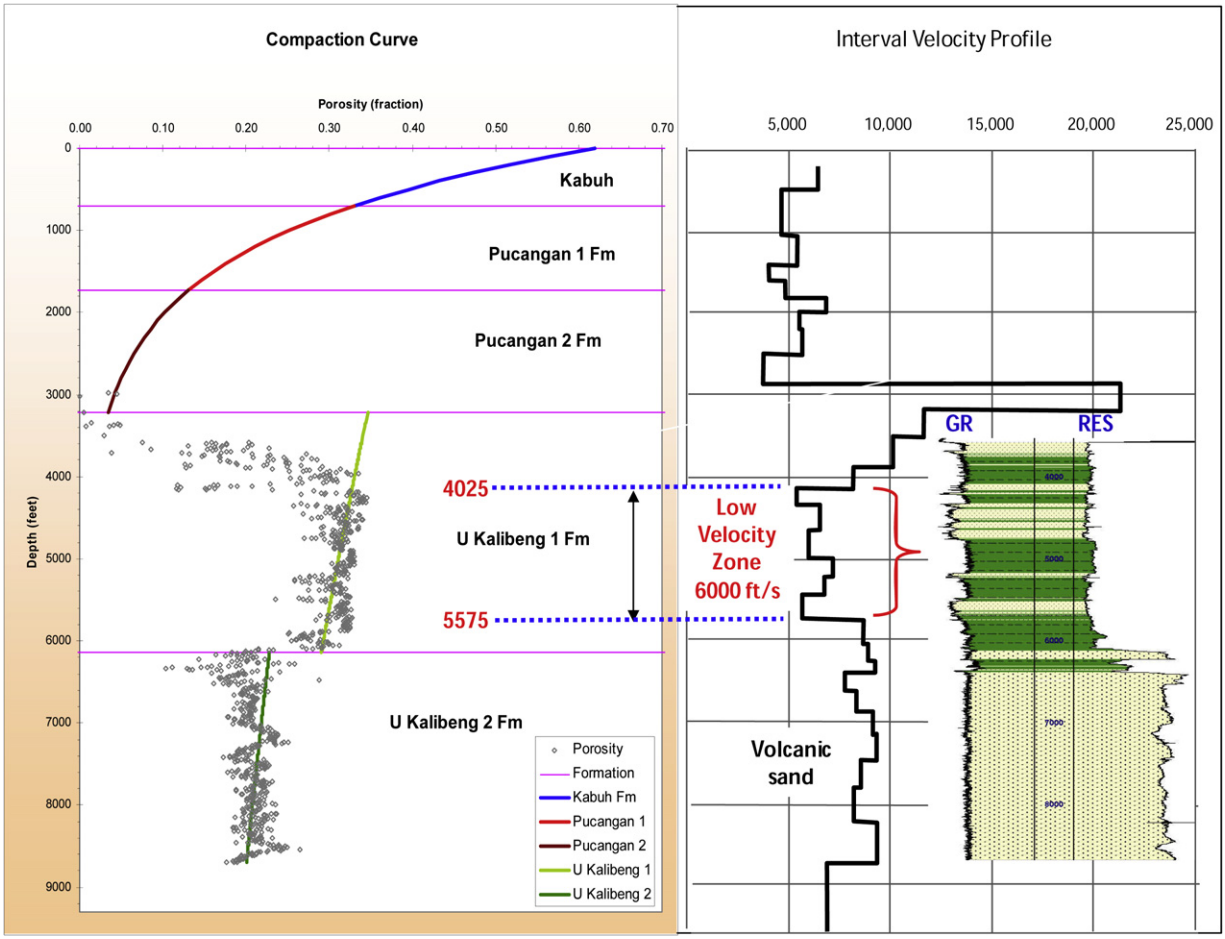

Fig. 8. Compaction curve of Banjarpanji-1 well showing the presence of under-compacted and over-pressured shale in the Upper Kalibeng 1 Formation. Seismically, it is a low-velocity zone as shown in the interval velocity profile. This zone is the source of mud, and its thickness was used to estimate the volume of mud that potentially might erupt.

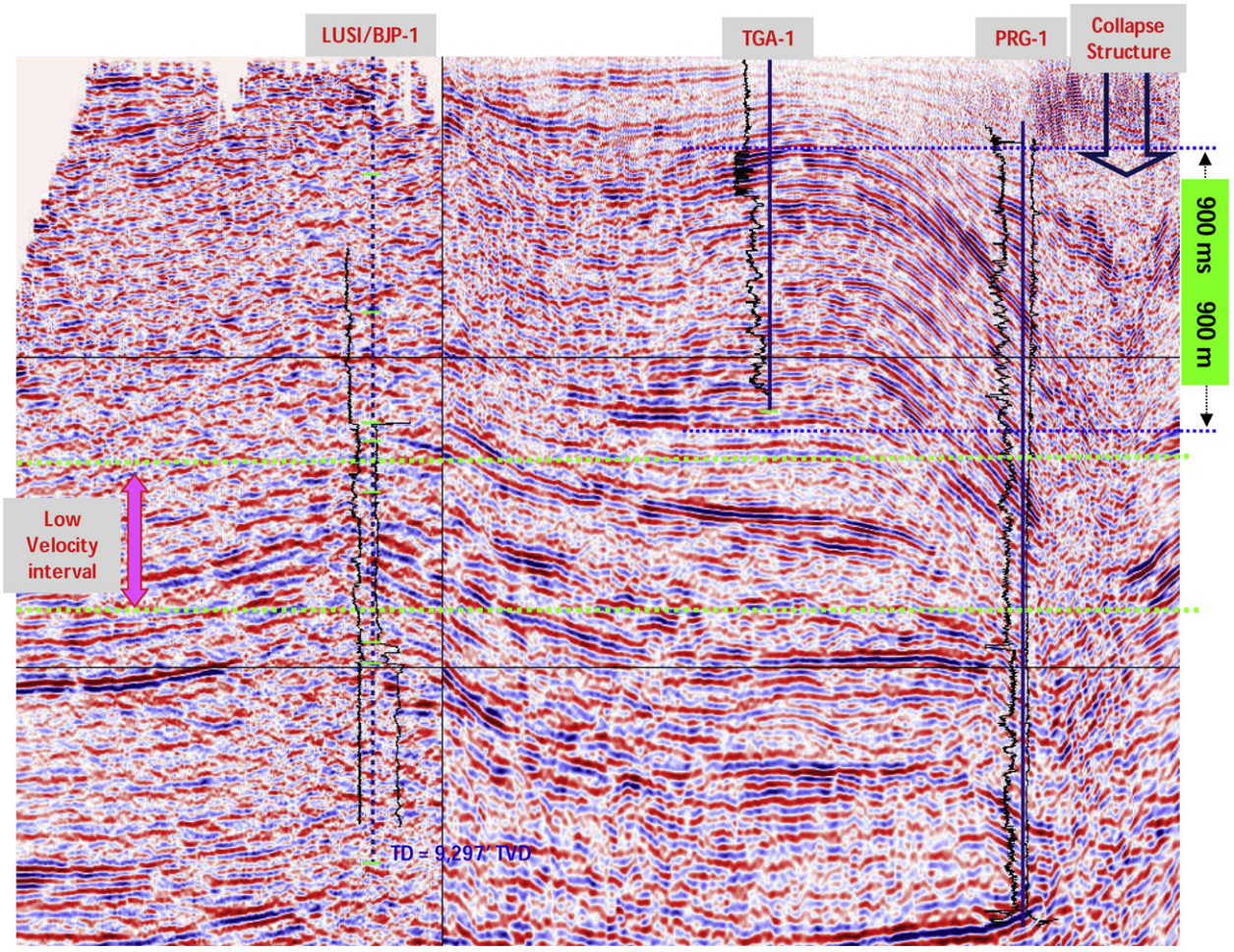

Fig. 9. Seismic section of LUSI – Banjarpanji-1 – Tanggulangin-1 – Porong-1 – Porong collapse structure. The Porong collapse structure located approximately 7 km from LUSI is a paleo mud volcano where subsidence is evident and the multiple faults present likely served as conduits for the mudflow. Similarly, the multiple faults near the BJP-1 well (200 m from LUSI) may have been reactivated and served as conduit for the mud eruptions and escaping gas, hence the appearance of gas bubbles along fault lines.

mud eruption rate was calculated by dividing the mud volume by the number of eruption days. This resulted in mud eruption rates of 50,785 m^3/day and 44,671 m^3/day for the months of June 2006 and July 2006 respectively, whilst the mud eruption rate from the May 2007 mud dimensions was 111,042 m^3/day, more than twice the rate in 2006. A mud eruption rate of 111,042 m^3/day was set for the initial runs in the model. This was varied for sensitivity analysis and history-matching with the satellite images. The IKONOS satellite image of January 2008 is the most recently available image to calibrate the model. When compared to the model prediction for December 2007, it was found that the mud rate of 111,042 m^3/day was too high. A rate of 90,000 m^3/day gave a closer match to the satellite images, so 90,000 m^3/day was used for subsequent predictions.

The lower mud rate needed to calibrate the model is consistent with the fact that after May 2007, mud started to be pumped into the Porong River. This was not accounted for in the early model runs. The pumping of mud out of the affected area was to reduce the mud burden. At the time of the writing, 10 pumps have been installed at various locations. When all the pumps are in operation, the combined pumping capacity is 190,000 m^3/day.

6.3. Subsidence

Subsidence continues as the mud eruption continues. The subsidence might result from any combination of ground relaxation due to mudflows, loading due to the weight of mud causing the area to compact, land settlement, geological structural transformation and tectonic activity (Abidin et al., 2007). The subsidence rate was obtained primarily from GPS measurements, while the extent of the subsidence was derived from InSAR data. The subsidence pattern is influenced by the fault system in the area.

The subsidence rates from GPS measurements from June 29, 2006 until April 12, 2007 were considered representative and so were used in the model. Periodic or continuous measurements could not be performed in all locations however due to the flooding of several monitoring stations. The highest subsidence magnitude of 5.53 cm/day was found near LUSI's main eruption vent, while the lowest rate of 0.04 cm/day was found just outside the predicted subsidence area from the InSAR image. Subsidence rates from periodical and continuous GPS measurements were extrapolated to the next time step by applying equations derived from second-order polynomial regression trend-lines. The model was populated with varying subsidence rates depending on the distance from the main mud eruption.

The subsurface expression and extent of subsidence is postulated to form a bowl or basin-like shape, resembling the Porong collapse structure 7 km away from the LUSI area (Figs. 9 and 10). The Porong collapse structure is a paleo mud volcano that shows crater, feeder pipe, multiple contemporaneous faults due to gravitational slumps and intrusive structure suggesting piercement from

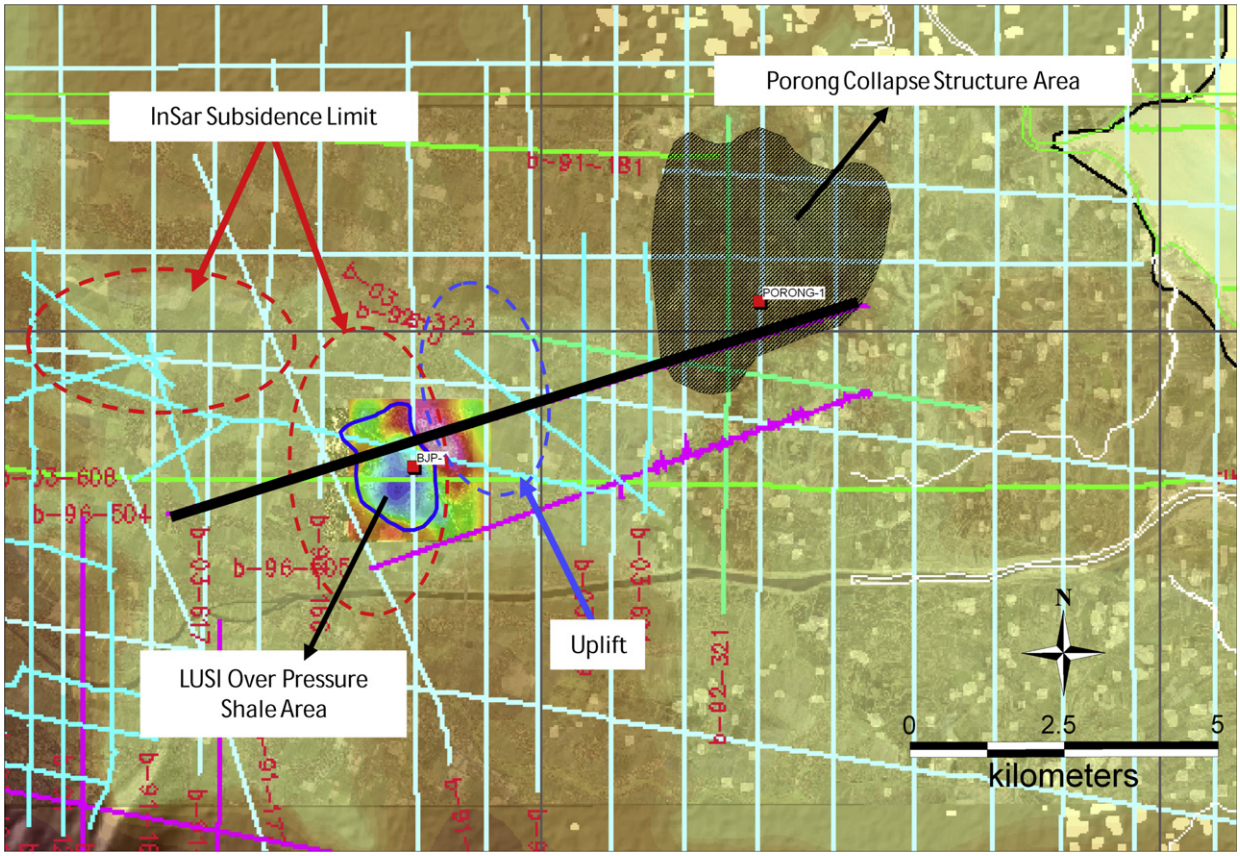

Fig. 10. Seismic base map overlays satellite image. The different colored lines represent the different seismic vintages and the black line is the seismic line of Fig. 9. LUSI area is defined by residual gravity map from Fig. 5. Note the areal extent of the Porong collapse structure in shaded dark color, which covers a much larger area compared to the LUSI interpreted over-pressured shale area. Porong is an adjacent mud volcano that was used as an analog to build the subsidence model for LUSI. (For interpretation of the references to color in this figure legend, the reader is referred to the web version of this article.)

the upward moving over-pressured sediments of the underlying shale diapir. This structure was used as an analog and reference in building the simulation model. The shape of the mud accumulation is assumed to have a semi-conical buildup with a peak around the main eruption vent. The assumption is based on mud volcano models developed by Kholodov (1983) and Kopf (2002) where LUSI is classified as a swampy mud volcano type. The peak will not be high due to the low viscosity of the extruding mud. The indicated oval shaped subsidence was applied in the model with intensity diminishing with distance. The subsidence bowl was rotated about 20° to the East to reflect the influence of the Watukosek fault (Fig. 3) which controls the fluid and mass remobilization (Fig. 6).

6.4. Fault parameters

Combining shallow fault information from VLF data with deformation information from GPS, gravity, microgravity and resistivity resulted in several observations which were considered in the subsidence pattern. The faults affected the subsidence through reactivation before and during the mud eruption. The observations were:

i. The West and Northwest areas have the highest deformation, controlled by cone depression and the fault system.
ii. The Northeast area has high deformation (8.3 cm vertical and horizontal movement in 22 days), controlled by the fault system.
iii. The South-East area has a lesser deformation (6.9 cm vertical and 7.2 cm horizontal movement in 22 days). This is a low gravity anomaly area, likely associated with mud withdrawal.

6.5. InSAR data

While GPS measurements provided the rate of subsidence and lateral movement at each monitoring point, they provided no information on areal extent. To overcome this limitation, satellite images were combined with GPS data to gain information on subsidence coverage. The images were recorded by a Synthetic Aperture Radar (SAR) PALSAR onboard the Japanese ALOS satellite (Advanced Land Observing Satellite). InSAR processing (Interferometric Synthetic Aperture Radar) of the affected area was studied (Deguchi et al., 2007; Fukushima et al., submitted for publication) in order to obtain continuous maps of ground displacements around LUSI.

The study indicated the shape of the subsiding area was oval with a maximum subsidence of 94 cm within 46 days or an average of 2 cm/day between October and November 2006. This rate is lower than the 3.9 cm/day rate obtained from GPS monitoring around the main mud eruption vent over the same period. The main reason for this difference is that InSAR cannot observe the area covered by mud, where a high subsidence rate is expected. It should also be noted that InSAR measures the displacements in the satellite looking direction, which was 49° from vertical, and that the value 1 m of subsidence has been obtained from a rough approximation of pure vertical subsidence (Fukushima, personal communication).

The area affected by subsidence is assumed to expand by 250 m over each 6-month period, based on multi-temporal Palsar Satellite data between May 2006 and February 2007 (Deguchi et al., 2007). Interferograms indicate subsidence in an ellipsoidal area of approximately 4 km (north–south) × 3 km (east–west), centered at

the main eruptive vent, due to pressure decrease and depletion of materials at depth (Fukushima et al., 2009).

6.6. Topography

The topographic map generated with a 1-m contour interval based on the 1:25,000 scale Bakosurtanal map spot-heights shows that the area surrounding LUSI is relatively flat. The elevation ranges from 6 m in the West to 1 m above mean sea level in the East. This relatively flat area implies that the mud will not easily flow to the sea by gravitational difference.

The flow direction in the model can be predicted if there are topographical controls. However, due to the relatively flat terrain, it is not easy to predict where the mud will flow in the future. The flow direction depends more on where the dikes are built and planned to be built, as they control, contain and constrain the spread of mud. Dikes prevent overflow to residential areas, villages and infrastructure such as roads and railways. The model assumes the dikes are continuously maintained, and new dikes are built if the existing dikes are not able to handle the volume of mud.

The mud buildup and dikes in the North force the mud to flow downhill to the South towards the Porong River. However if these dikes fail, then the mud will flow to the North. Some mud will naturally flow to the East as the area generally dips gently to the East-NE.

6.7. Results

The initial mud volume in the model was 37.3 million m^3 from the most recent survey data (May 2007). The simulation model was calibrated at the December 2007 time step by adjusting the mudflow rate until the flooded area matched the satellite images from the same period (Fig. 7). The spread of the mudflow was then simulated from December 1, 2007 to June 1, 2010 in 6-month time step.

The cumulative mud volume at a future date can be computed from the present mud volume and the predicted mud rate. The figure below illustrates the mud volume calculation.

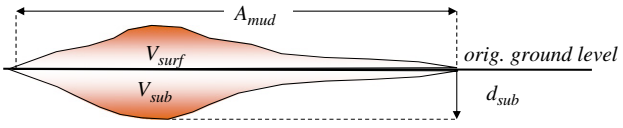

The calculated total volume consists of the volume below (V_{sub}) and above (V_{surf}) the pre-subsidence original ground level:

$$V_{total} = V_{sub} + V_{surf} \quad (3)$$

The simulated total volume is obtained from the initial mud volume (V_{init}), mud discharge (Q_{mud}) and elapsed time (t):

$$V_{total} = V_{init} + (Q_{mud} * t) \quad (4)$$

where the initial mud volume is 37.3 million m^3 and the mudflow rate is 90,000 m^3/day.

The subsurface portion is the subsidence volume computed from the total subsiding area (A_{mud}) multiplied by depth (d_{sub}):

$$V_{sub} = A_{mud} * d_{sub} \quad (5)$$

while the depth depends on rate of subsidence (r_{sub}):

$$d_{sub} = r_{sub} * t \quad (6)$$

The subsidence rate for each five-by-five meter grid cell was interpolated from subsidence rates from GPS using the nearest-neighbor approach. Each grid cell volume was computed using the cut-and-fill function in the GIS software package. The surface volume portion (V_{surf}) was the difference between the total volume and the subsidence volume. Several scenarios were applied, such as the increasing dike height and allowing mud spill into new areas.

The simulated mud areas and volumes until June 2010 are shown in Table 1. For every six-month period, the expansion of area covered by mud was predicted to be between 25 and 292 hectares. The continuous increase in mud volume was due to the application of a constant mud discharge. By June 2010, the predicted mud volume was 136 million m^3 and the maximum affected area was 1448 hectares.

Fig. 11 shows the possible areas affected by mud. From December 2007 and June 2008, the mud could spread eastward since this area is relatively flat and does not have significant infrastructure. Flooding could also occur in the western area. The highway and railway are on this side, so priority should be given to maintain the western dikes. The simulation results show that the mud will not expand to the north, and will be limited to the south by the river. By December 2008, the mud could start flooding the western area where the intercity highway and railway run. The western dikes must be strengthened to hold the mud and prevent the flooding of the highway and railway. By June 2009, several kilometers of highway could be inundated by mud. It is recommended that an alternative highway and railroad route be prepared to avoid loss of accessibility due to the mud flood. A more recent reality check update in December 2008 showed that the mudflow did not flood the intercity highway and railway as a result of the suggested strengthening of the western dikes.

Fig. 12 shows the predicted evolution of the cross-sectional view. The peak is relatively stable at 21 m and reaches a maximum height of 26 m near LUSI's main eruption vent. The high subsidence rate around the main eruption vent is reflected by the sinking of the original pre-subsidence surface by up to −63 m by June 2010. The subsidence rate is predicted to be 9 m per six months until December 2008, thereafter decreasing slightly to 8 m per six months until June 2010.

Fig. 13 shows the predicted spread of the subsidence area. The affected area is predicted to grow from 4.1 by 6.4 km in December 2007 to approximately 6.4 by 8.4 km by June 2010.

6.8. Model limitation

The mud growth model is as valid as the assumptions used to build it. Although numerous data sets were used to control the model, some discrepancies between the prediction and reality may occur, as many assumptions were used to control the simulation. The two important parameters which were assumed to be correct were the eruption rate and the subsidence rate which set the boundary conditions and constrain the behavior of the mudflow model. Incorrect assumptions will lead to an unrealistic representation of the real condition, and therefore erroneous predictions of affected areas. The eruption rate and the subsidence rate used in the mud growth model were both estimated from reliable data.

Table 1
Future area and volume of mud.

Date	Area (hectares)	Volume (millions m^3)
December 1, 2007	832	54
June 1, 2008	960	70
December 1, 2008	1252	87
June 1, 2009	1393	103
December 1, 2009	1418	119
June 1, 2010	1448	136

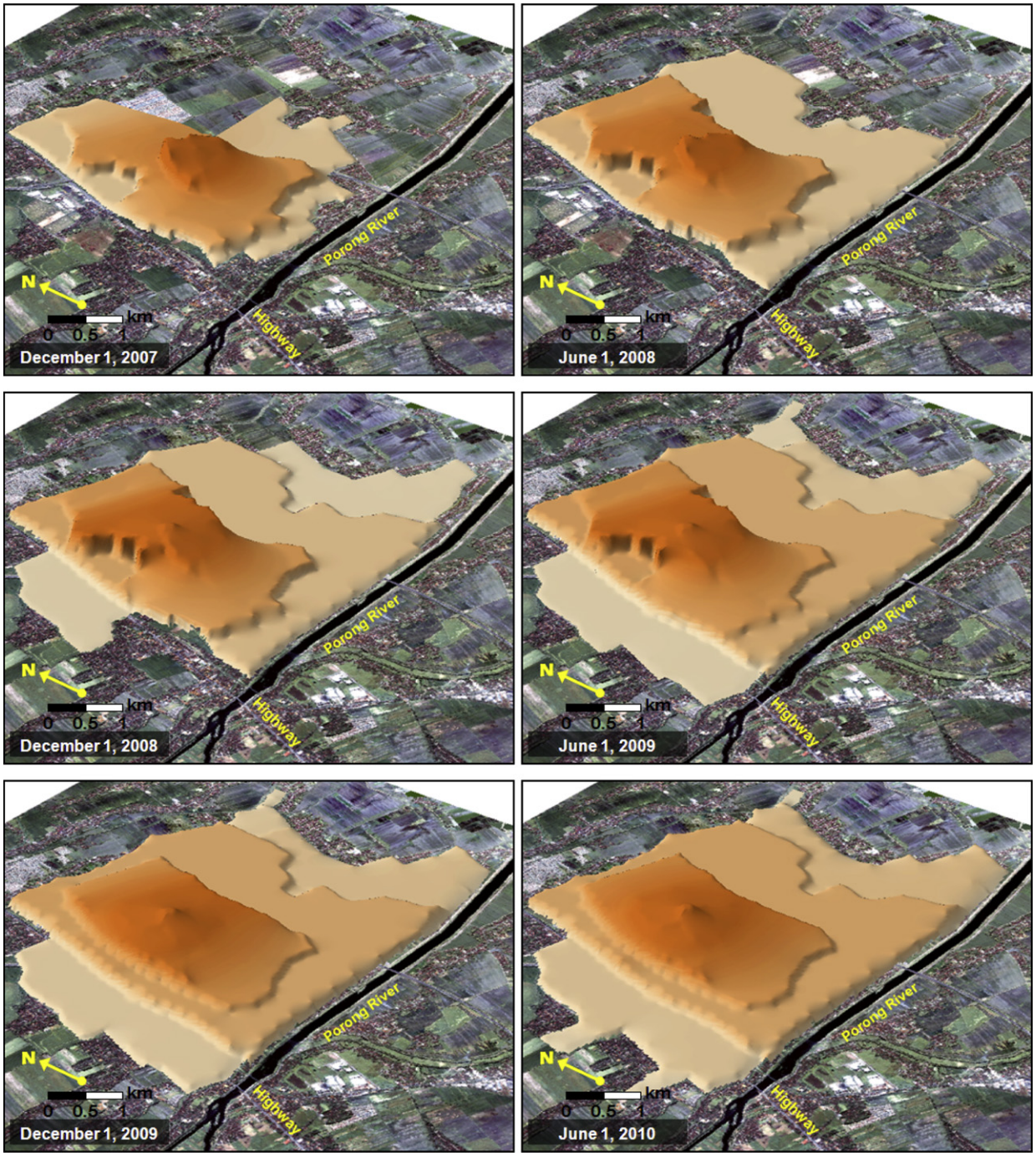

Fig. 11. Predicted mud growth from December 2007 to June 2010. Note the wide mud spread to the east and west, due to the low mud viscosity and relatively flat topography. The mud spread to the north and south is hindered by the presence of river dikes.

The model however, needs to be reviewed periodically as the mud eruption is very dynamic. For example there are indications of accelerated exponential, non-linear concentric subsidence pointing towards eruption then rebound in some peripheral areas. Eruption rates also increase two-to-three-fold after every earthquake within 300 km with $M > 3.7$ (Mazzini et al., 2007). Therefore the model has to be adjusted periodically to honor horizontal and vertical displacements which have spatial and temporal variations in magnitude and direction.

Measures in controlling the spread of mud from its natural path have resulted in variance of the predicted affected areas. For example, building new dikes, strengthening existing dikes and mud disposal to the river may prevent the predicted mud floods. On the other hand, the instability of the soil and pebble dikes may result in dike breakdown and overspill. Other factors include land displacement (compaction, horizontal movement and subsidence) and high rainfall. Never-the-less, the model prediction for August to December 2006 with a one-month time step closely matched reality (Pramono and Poniman, 2007).

7. Conclusions

A natural 'mud-volcano' is being formed at the LUSI site, based on analysis of mudflow movement along fault planes, the presence

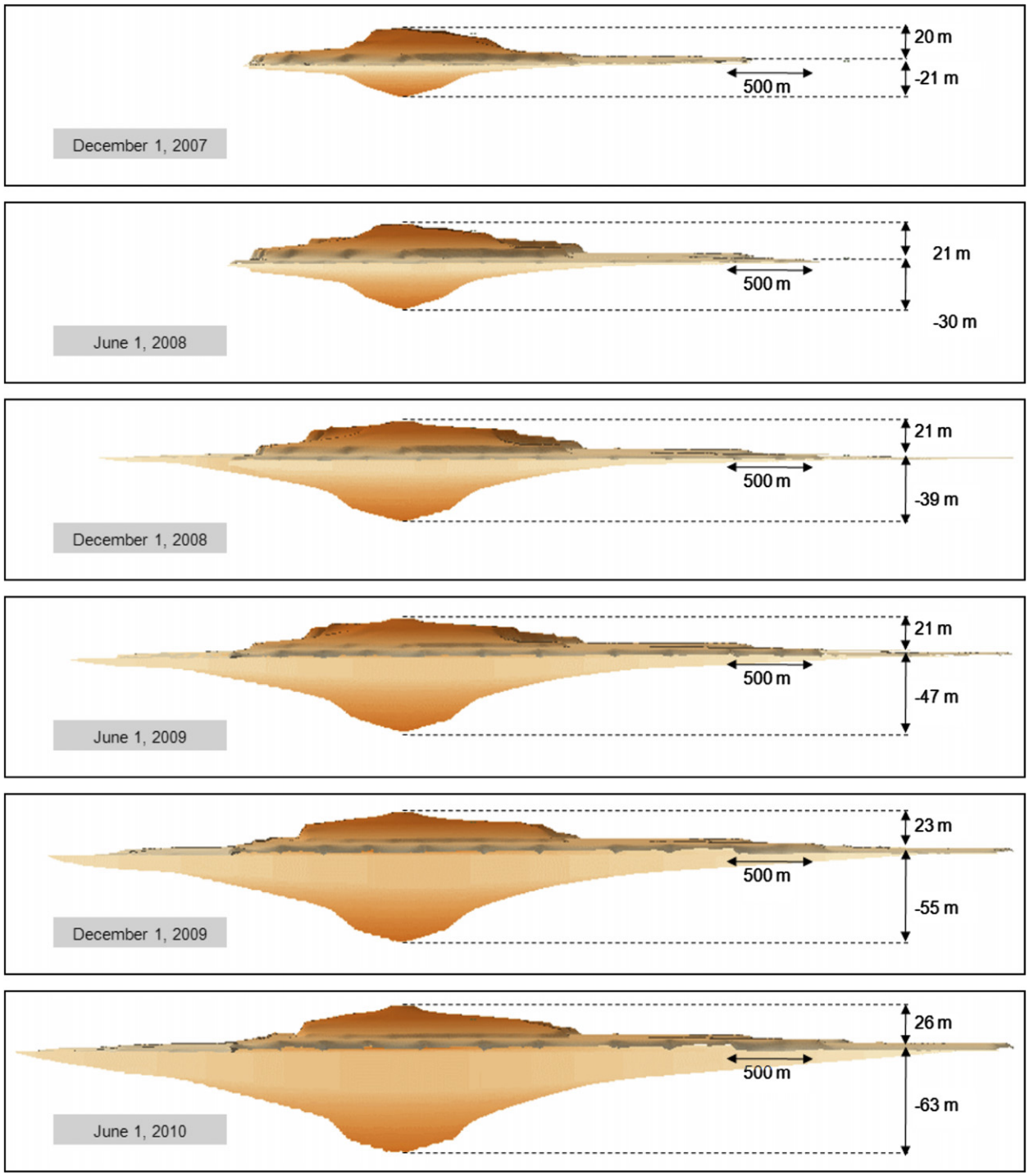

Fig. 12. Cross-sectional view from the South showing the predicted mud growth and subsidence from December 2007 to June 2010. The greatest subsidence is found near the main mud eruption vent, and it forms a depression-cone-like structure.

of many mud volcanoes in the area, and the huge quantity of mud being erupted. The constant tectonic movement will strain and potentially shear surface structures and infrastructures, damaging houses and dikes, causing mud flooding. Vertical and horizontal movement may further damage infrastructure, particularly railroads and gas and water pipelines. The continued reactivation of faults and the formation of fractures and fissures will cause the emergence of more gas bubbles within a radius of 2–3 km from the main mud eruption vent along weak lineaments.

There is no possibility to stop the mud eruption. Drilling of new relief wells to stop the mudflow is not viable. Severe problems will arise on any future relief wells. Movement will cause instability of rig equipment, location, casing collapse and bucking of drill strings. New relief wells will likely experience continuous loss and kick situations and will likely experience pressure losses in the casing (casing leaks) and tight hole due to the movements. There is no obvious location from which to drill a relief well. Drilling from outside the subsidence area is not practical as the horizontal

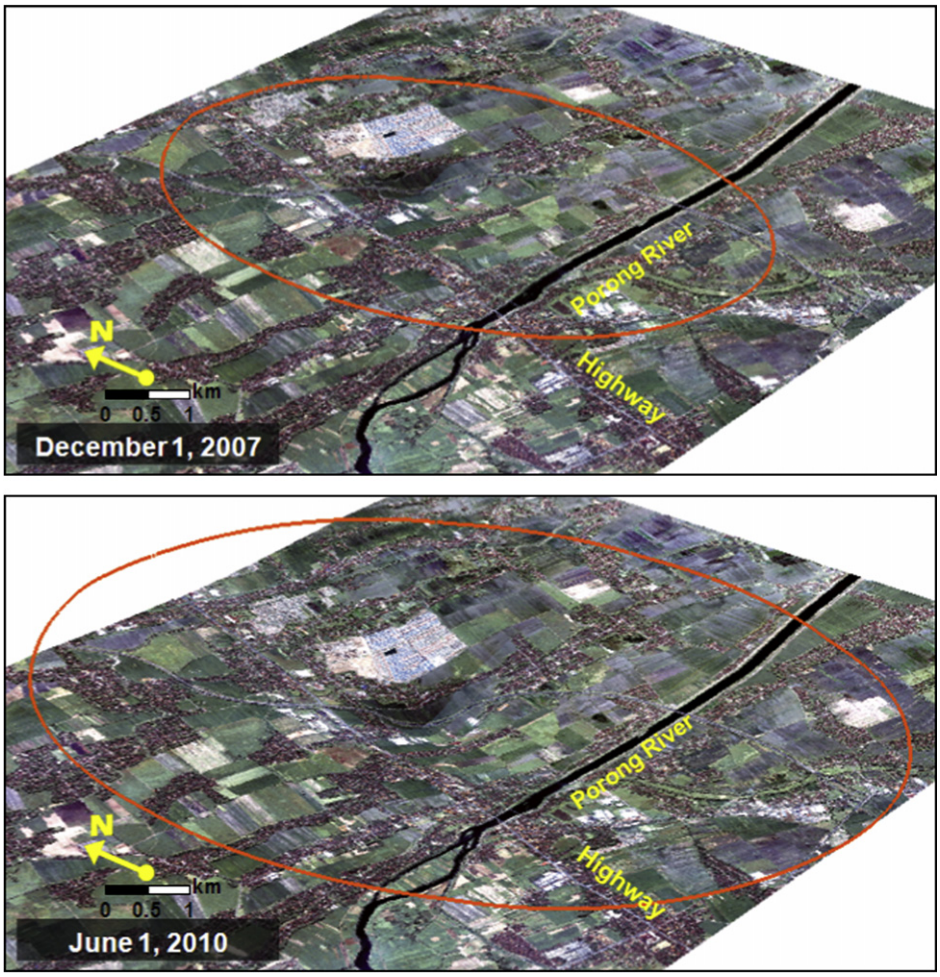

Fig. 13. The ongoing subsidence, while it forms an accommodation space to naturally contain the mud but is also causing damage. The progression of the subsiding area is shown by the red circle. It is 6.4 km wide from north to south in the December 2007 simulation. By June 2010, it is predicted to expand to 8.4 km. Areas that are protected by dikes may not be inundated by mud but will experience subsidence in the future. Many more houses in the subsiding areas will be damaged (e.g. wall cracks) due to the movements during subsidence process.

displacement is too great. If the mud eruption does stop in one location, it is likely to emerge in another location(s) along the Watukosek fault zone. The mudflow will naturally stop when equilibrium is reached between the subsurface mass and pressure.

Given the low probability of success of relief well(s) efforts, the high expense due to the potential problems mentioned above and the safety of the operation, the recommendation is to not drill relief well(s), but instead continue predicting the mudflow extent and the areas which could be affected by the ongoing mud eruption and subsidence. This would enable pro-active remediation of potential problems to the community, infrastructure and the environment.

A three-dimensional simulation model was built to predict the timing and extent of damage to local infrastructure. The simulation model employs a Geographic Information Systems (GIS) approach. Inputs for the model came from several data sets. The model was calibrated using actual mud area and spill data and satellite images for August–December 2006. In prediction mode, the model estimates the magnitude and timing of mud volcano growth and land subsidence. Periodical surveillance in areas designated as vulnerable to geohazard risks is needed to update the model, in particular in identified reactivated faulted areas along the axis of the Watukosek lineament and its conjugate faults. Mud discharge, subsidence, and collapse of dike are dynamic data, so newly available data should be integrated to the model to achieve a realistic prediction.

Acknowledgements

The authors express appreciation to the management of BPMIGAS, Lapindo Brantas Inc. and its partners for permission to publish the paper as well as Bakosurtanal, ITB, ITS, LAPI, IAGI in particular Dr. Edy Sunardi for his support and cooperation during the surveys, studies and in understanding the LUSI phenomena. Colleagues at EMP – TCC, BPLS and Lapindo are also appreciated. The authors wish to pay a special tribute to the late Dr Seno Sardjono who was a member of the LUSI assessment team.

References

Abidin, H.Z., Kusuma, M.A., Istadi, B., Darmoyo, A.B., Sumintadireja, P., Purwaman, I., Andreas, H., Gamal, M., 2007. GPS-based monitoring of subsidence phenomenon in the mud extrusion areas, Sidoarjo, East-Java. In: Proceedings of the International Union of Geodesy and Geophysics (IUGG) XXIV, Perugia, Italy.

Allis, R.G., Hunt, T.M., 1986. Analysis of exploration induced gravity changes at Wairakei geothermal field. Geophysics 51, 1647–1660.

Davies, R., Swarbrick, R., Evans, R., Huuse, M., 2007. Birth of a mud volcano: East Java, 29 May 2006. GSA Today 17, 4–9.

Davies, R.J., Brumm, M., Manga, M., Rubiandini, R., Swarbrick, R., Tingay, M., 2008. The East Java mud volcano (2006 to present): an earthquake or drilling trigger? Earth and Planetary Science Letters 272, 627–638.

De Genevraye, P., Samuel, L., 1972. Geology of the Kendeng zone (Central and East Java). In: Proceedings of the Indonesian Petroleum Association, 1st Annual Convention, pp. 17–30.

Deguchi, T., Maruyama, Y., Kato, M., Kobayashi, C., 2007. Surface displacement around mud volcano, East Java captured by Insar using Palsar data. In: Proceedings of the 28th Asian Conference on Remote Sensing.

Fukushima, Y., Mori, J., Hashimoto, M., Kano, Y., 2009. Subsidence associated with the LUSI mud eruption, East Java, investigated by SAR interferometry. Journal Marine and Petroleum Geology 26, 1740–1750.

Gafoer, S., Ratman, N., 1999. Peta Geologi Regional Jawa Bagian Timur, Skala 1:500.000. Pusat Penelitian dan Pengembangan Geologi, Bandung.

Hall, R., 2002. Cenozoic geological and plate tectonic evolution of SE Asia and the SW Pacific: computer based reconstructions, model and animations. Journal of Asian Earth Sciences 20, 353–432.

Hamilton, W.R., 1979. Tectonics of the Indonesian Region. US Geological Survey Professional Paper 1078. US Government Printing Office.

Hogan, C.M., 1973. Analysis of highway Noise. Journal of Water, Air, & Soil Pollution 2 (3), 387–392. Biomedical and Life Sciences and Earth and Environmental Science Issue, Springer Verlag, Netherlands.

Issler, D.R., 1992. A new approach to shale compaction and stratigraphic restoration, Beaufort–Mackenzie Basin and Mackenzie Corridor, Northern Canada. AAPG Bulletin 76, 1170–1189.

Istadi, B.P., Kadar, A., Sawolo, N., 2008. Analysis & recent study results on East Java mud volcano. In: Proceedings of the Subsurface Sediment Remobilization and Fluid Flow in Sedimentary Basin Conference, October 2008. The Geological Society, Burlington House, Piccadilly, London.

Jentzsch, G., Calvache, M., Bermudez, A., Ordonez, M., 1999. Microgravity and GPS at Galeras volcano, Columbia: establishment of a new network and first measurements. In: Abstract for the International Symposium on Andean Geodynamics, Göttingen, October 1999.

Kadar, A.P., Kadar, D., Aziz, F., 2007. Pleistocene stratigraphy of Banjarpanji#1 well and the surrounding area. In: Proceedings of the International Geological Workshop on Sidoarjo Mud Volcano, Jakarta, IAGI-BPPT-LIPI, February 20–21, 2007. Indonesia Agency for the Assessment and Application of Technology, Jakarta.

Karous, M., Hjelt, S.E., 1985. Linear filtering of VLF dip angle measurements. Geophysical Prospecting 31 (5), 782–794.

Kholodov, V.N., 1983. Formation of gas–water fluids in sandy–clayey deposits of Elision Basins. In: Sedimentary Basins and their Oil–Gas Potential. Nauka, Moscow, pp. 28–44 (in Russian).

Kopf, A.J., 2002. Significance of mud volcanism. Reviews of Geophysics 40, 1–52.

Mazzini, A., Svensen, H., Akhmanov, G.G., Aloisi, G., Planke, S., Malthe-Sørenssen, A., Istadi, B., 2007. Triggering and dynamic evolution of the LUSI mud volcano, Indonesia. Earth and Planetary Science Letters 261, 375–388.

Pendrod, K., Ellsworth, A., Farrel, J., 2006. Application of GIS to Estimate the Volume of the Great Johnstown Flood. http://www2.nature.nps.gov/ParkScience/index.cfm?ArticleID=74 (7 December 2006).

Pramono, G.H., Poniman, A., 2007. The validation of mud flow model using multi-temporal satellite images. In: Proceedings of the 28th Asian Conference on Remote Sensing, Kuala Lumpur, Malaysia.

Pramono, G.H., Sardjono, S.P., 2007. The application of geographic information systems to measure mud dimension in Porong, Sidoarjo. Forum Geografi 21 (2).

Prasetyadi, C., Suparka, E.R., Harsolumakso, A.H., Sapiie, B., 2006. The occurrence of a newly found Eocene tectonic Melange in Karangsambung Area, Central Java. In: Proceedings of the IAGI 35th Annual Meeting and Exhibition, Pekanbaru, October 2006.

Price, M., October–December 2002. Deriving Volume with ArcGIS Spatial Analyst. ArcUser, pp. 53–56.

Reynolds, J.M., 1997. An Introduction to Applied and Environmental Geophysics. John Wiley & Sons Ltd., England, p. 428.

Sawolo, N., Sutriono, E., Istadi, B.P., Darmoyo, A.B., 2008. East Java mud volcano (LUSI): drilling facts and analysis. In: Proceedings of the African Energy Global Impact, AAPG International Conference and Exhibition, October 2008, Cape Town, South Africa.

Sawolo, N., Sutriono, E., Istadi, B.P., Darmoyo, A.B., 2009. Mud volcano triggering controversy: was it caused by drilling? Journal Marine and Petroleum Geology 26, 1766–1784.

Schiller, D.M., Seubert, B.W., Musliki, S., Abdullah, M., 1994. The reservoir potential of globigerinid sands in Indonesia. In: Proceedings of the 23rd Annual Convention, Proceedings of the Indonesian Petroleum Association, vol. 1, p. 189ff.

Sclater, J.G., Christie, P.A.F., 1980. Continental stretching: an explanation of the post-Mid-Cretaceous subsidence of the Central North Sea Basin. Journal of Geophysical Research 85 (B7), 3711–3739.

Smyth, H., Hall, R., Hamilton, J., Kinny, P., 2005. East Java: Cenozoic Basins, volcano and S–N cross section line ancient basement. In: Proceedings of the 13th Annual Convention & Exhibition. Indonesian Petroleum Association.

Sribudiyani, Prasetya, I., Muchsin, N., Sapiie, B., Ryacudu, R., Asikin, S., Kunto, T., Harsolumakso, A.H., Astono, P., Yulianto, I., 2003. The collision of the East Java microplate and its implication for hydrocarbon occurrences in the East Java Basin. In: 29th Annual Convention Proceedings of the Indonesian Petroleum Association.

Sumintadireja, P., Purwaman, I., Istadi, B., Darmoyo, A.B., 2007. Geology and geophysics study in revealing subsurface condition of Banjarpanji mud extrusion, Sidoarjo, East Java, Indonesia. In: Proceedings of the International Union of Geodesy and Geophysics (IUGG) XXIV, Perugia, Italy.

Talwani, M., Worzel, J.L., Landisman, M., 1959. Rapid gravity computation for two-dimensional bodies with application to the Mendocino submarine fracture zone. Journal of Geophysical Research 64 (1), 49–59.

Tingay, M., Heidbach, O., Davies, R., Swarbrick, R., August 2008. Triggering of the Lusi mud eruption: earthquake versus drilling initiation. Geology 36 (8), 639–642.

van Bemmelen, R.W., 1949. General Geology of Indonesia and Adjacent Archipelagos. In: The Geology of Indonesia, vol. IA. Martinis Nijhoff, The Hague, 732 pp.

Willumsen, P., Schiller, D.M., 1994. High quality volcaniclastic sandstone reservoirs in East Java, Indonesia. In: 23rd Annual Convention, vol. I. IPA, pp. 101–111.